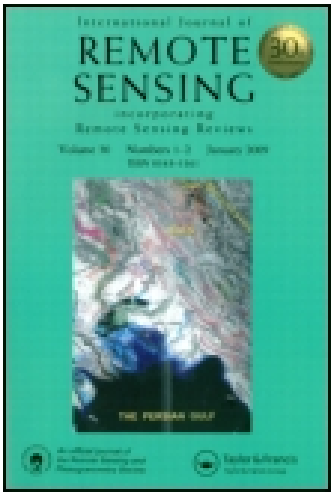

International Journal of Remote Sensing

Publication details, including instructions for authors and subscription information:
http://www.tandfonline.com/loi/tres20

Detection of collapsed buildings caused by the 1999 Izmit, Turkey earthquake through digital analysis of post-event aerial photographs

M. Turker [a] & B. T. San [b]

[a] Graduate School of Natural and Applied Sciences Geodetic and Geographic Information Technologies , Middle East Technical University , Ankara, 06531, Turkey E-mail:

[b] Graduate School of Natural and Applied Sciences Geodetic and Geographic Information Technologies , Middle East Technical University , Ankara, 06531, Turkey E-mail:

Published online: 26 Nov 2010.

To cite this article: M. Turker & B. T. San (2004) Detection of collapsed buildings caused by the 1999 Izmit, Turkey earthquake through digital analysis of post-event aerial photographs, International Journal of Remote Sensing, 25:21, 4701-4714, DOI: 10.1080/01431160410001709976

To link to this article: http://dx.doi.org/10.1080/01431160410001709976

INT. J. REMOTE SENSING, 10 NOVEMBER, 2004,
VOL. 25, NO. 21, 4701–4714

Taylor & Francis
Taylor & Francis Group

Detection of collapsed buildings caused by the 1999 Izmit, Turkey earthquake through digital analysis of post-event aerial photographs

M. TURKER* and B. T. SAN

Middle East Technical University, Graduate School of Natural and Applied Sciences, Geodetic and Geographic Information Technologies, 06531 Ankara, Turkey; e-mail: mturker@metu.edu.tr, tanersan@mta.gov.tr

(*Received 15 July 2003; in final form 15 January 2004*)

Abstract. In this study, the post-earthquake aerial photographs were digitally processed and analysed to detect collapsed buildings caused by the Izmit, Turkey earthquake of 17 August 1999. The selected area of study encloses part of the city of Golcuk, which is one of the urban areas most strongly hit by the earthquake. The analysis relies on the idea that if a building is collapsed, then it will not have corresponding shadows. The boundaries of the buildings were available and stored in a Geographical Information System (GIS) as vector polygons. The vector building polygons were used to match the shadow casting edges of the buildings with their corresponding shadows and to perform analyses in a building-specific manner. The shadow edges of the buildings were detected through a Prewitt edge detection algorithm. For each building, the agreement was then measured between the shadow producing edges of the building polygons and the thresholded edge image based on the percentage of shadow edge pixels. If the computed percentage value was below a preset threshold then the building being assessed was declared as collapsed. Of the 80 collapsed buildings, 74 were detected correctly, providing 92.50% producer's accuracy. The overall accuracy was computed as 96.15%. The results show that the detection of the collapsed buildings through digital analysis of post-earthquake aerial photographs based on shadow information is quite encouraging. It is also demonstrated that determining the optimum threshold value for separating the collapsed from uncollapsed buildings is important.

1. Introduction

A strong earthquake of magnitude 7.4 struck north-west of Turkey on 17 August 1999 causing tremendous damage in urban areas of Golcuk, Yalova, Izmit and Istanbul, killing more than 17 000 people and damaging thousands of buildings. The epicentre (40.75° N, 29.86° E, USGS) was near the city of Izmit, at the eastern end of Izmit Bay, which is an east–west elongated structural basin situated along the North Anatolian fault at the eastern margin of the Sea of Marmara (figure 1). The region is in the first-degree earthquake zone. Nearly 20% of the total population live in this region. Most of the industrial complexes and power plants are also established in this region.

*Corresponding author.

International Journal of Remote Sensing
ISSN 0143-1161 print/ISSN 1366-5901 online © 2004 Taylor & Francis Ltd
http://www.tandf.co.uk/journals
DOI: 10.1080/01431160410001709976

Figure 1. The study area, north-west Turkey.

This strong earthquake caused extensive damage to buildings, facilities and lifelines, dramatically changing the land surface of the damaged region. Most of the damage during the earthquake resulted from strong ground shaking. The fault rupture also contributed directly to complete collapse or significant damage of apartment buildings and houses (Lettis *et al.* 2000). The detection of the collapsed buildings due to such a destructive event is a vital issue for rescue operations. Fast and reliable information about the location, extent and level of damage of the hard-hit areas, particularly urban areas, is important for the rescue planning actions. Of course, an accurate damage assessment can be conducted through a field reconnaissance survey. However, this may require a long time and a lot of resources. After such a destructive earthquake, a fast assessment of the collapsed buildings is required for rescue operations and dispatching the rescue teams. Space and aerial images acquired after the occurrence of an earthquake have become an excellent data source for the detection and assessment of the hard-hit areas. Recent developments in image processing and analysis techniques have made it possible to detect damages and changes caused by the earthquake through automated analysis of the images.

2. Past studies

Several studies using satellite and aerial images have been performed to detect earthquake-induced damages and changes. Gupta *et al.* (1994) used pre- and post-earthquake remote sensing datasets of the Uttarkashi area for detecting earthquake-induced damage by applying an image differencing change detection technique. Gamba and Casciati (1998) developed a system that contains a two-phase operating model for earthquake-damage assessment by image-processing tools and Geographical Information System (GIS) integration within a single user interface environment. In the pre-event era, images and data about buildings are collected and analysed. Immediately after the earthquake, the system receives near-real-time images of the affected area and compares them with the pre-event dataset. They

applied the procedure to aerial photos and satellite images taken before and after different hazards and reported satisfactory results. Saraf *et al*. (2002) mapped Kutch earthquake-induced damage to houses and liquefaction-affected regions by applying a pseudo-colour transform technique to pre- and post-earthquake Indian Remote-sensing Satellite (IRS)-1C/D datasets. Singh *et al*. (2002) used multi-sensors (IRS-P4–Ocean Color Monitor (OCM) and IRS-1D–Linear Imaging Self-scanning Sensor (LISS)-III) and multi-date remote sensing datasets to show the changes in land and ocean. While the changes in land were detected through band rationing of pre- and post-event IRS-1D–LISS-III datasets, the changes along the coastline were detected through visual comparison of pre- and post-quake IRS-P4–OCM datasets. Recently, Turker and San (2003) detected the 1999 Izmit earthquake-induced changes by subtracting the near-infrared channel (band 3) of the merged pre-quake Système Probatoire de l'Observation de la Terre (SPOT) high-resolution visible (HRV) (XS and PAN) image from that of the merged post-quake SPOT HRV (XS and PAN) image. The overall accuracy for the change areas was computed as 83%. In addition, the detailed analysis was performed to detect the damaged building blocks within a selected hard-hit urban area. The results reveal that the building blocks that contain the collapsed buildings can be detected and categorized according to predefined damage conditions. Further, Turker and Cetinkaya (in review) detected the collapsed buildings caused by the 1999 Izmit earthquake using digital elevation models (DEMs) created from the aerial photographs taken before (1994) and after (1999) the earthquake. The DEMs created from two epochs were differenced and the difference DEM was analysed building by building to detect those buildings whose height difference between pre- and post-earthquake exceeds a specified threshold. The producer's accuracy for collapsed buildings was computed as 84%. It was concluded that the difference DEM of the pre- and post-earthquake aerial photographs can successfully reveal the collapsed buildings caused by the earthquake.

3. The objective

The objective of this study was to detect collapsed buildings caused by the earthquake through digital analysis of post-event aerial photographs. One important property of buildings, particularly multi-storey buildings, is that when illuminated by the Sun, they cast shadows. In this study, we show how the relationship between the buildings and the cast shadows is exploited to detect collapsed buildings due to earthquake. In several studies, the shadow information has been used for building detection since the presence of shadows in an urban scene indicates the existence of buildings (Huertas and Nevatia 1988, Irvin and McKeown 1989, Liow and Pavlidis 1990, Lin *et al*. 1994). Shadows may cause problems in image analysis; here we use the shadows to our advantage for detecting the collapsed buildings due to earthquake. The analysis relies on a basic idea that if a building is collapsed then it will not have corresponding shadows. Therefore, the analysis of the shadow edges can provide very useful cues for detecting, up to a certain extent, the collapsed buildings. The building boundaries are available and stored in a GIS as vector polygons. The vector boundaries are used to match the shadow casting edges of the buildings with their corresponding shadows and to perform assessments in a building-specific manner. The advantage of the building-based assessment logic is that, for each building, only the corresponding shadow edge pixels are included in the assessment of the building. Therefore, those edge

pixels falling outside the building polygons do not affect the assessment results. The Sun angle, relative to aerial image, is also known *a priori*.

4. The study area and data description

The selected area of study (figure 1) encloses part of the city of Golcuk, which is one of the urban areas most strongly hit by the earthquake. It is located on the south coast of Izmit Bay and encompasses an area of approximately 1 km × 0.8 km. The Sea of Marmara is located on the western part of Golcuk. The Bursa–Istanbul highway extends from east to west, dividing the city into two halves. While the majority of the urban structures are located between the Sea of Marmara and the Bursa–Istanbul highway, widely spaced single dwellings are observed mostly in the southern part of the highway. The selected urban area contains a significant number of collapsed and partially damaged multi-storey apartment buildings (figure 2). Therefore, these characteristics make the area interesting and challenging for detecting the collapsed buildings caused by the Izmit earthquake through digital analysis of the post-event aerial photographs.

In September 1999, General Command of Mapping (GCM) took 4000 black and white aerial photographs (1 : 16 000 scale), which cover about 12 000 km^2 in the region, to determine the damages caused by the earthquake, to use them in regional and city planning, and to rebuild new urban areas. GCM is a national mapping agency of Turkey in charge of the production and revision of 1 : 25 000 and smaller-scale topographic maps for both national defence and development purposes. GCM scanned the aerial photographs at 21 μm resolution using a Zeiss Scai photogrammetric scanner and produced approximately 1300 (1 : 5000 scale) digital orthophotos with 0.5 m resolution. The digital orthophoto corresponding to the study area was therefore obtained from GCM to perform digital processing and analysis operations for the damage detection. In addition to the digital orthophoto, one

Figure 2. The post-earthquake digital orthophoto of the selected urban area.

sheet of 1 : 5000-scale paper map generated through ground surveying in 1998 was also available. This map was used to digitize the boundaries of the buildings.

5. Methodology

5.1. *Pre-processing*

Data processing and analysis operations were carried out using PCI GEOMATICA Image Analysis System (PCI 2002). The selected urban area consists of four- to six-storey rectangular-shaped apartment blocks. In order to make the assessments in a building-specific manner, a total of 467 buildings falling within 85 building blocks were manually digitized from the map and stored as vector polygons. To select the polygons through a database query, each polygon was assigned a unique identification number. The edges of each building polygon were also given numerical codes starting from 1 for the first edge and increasing consecutively in a clockwise direction. For example, if a building polygon has four edges, the first edge is assigned 1, and the remaining three edges are assigned 2, 3 and 4 in a clockwise direction, respectively. Such a labelling process of the edges was necessary to identify the shadow producing edges of a building being assessed and to match these edges with the corresponding shadows.

The digital orthophoto was filtered using Gaussian smoothing and Prewitt edge filters. In both filtering techniques 3×3 kernels were used to compute the filtered value. First, a Gaussian filter was applied to smooth the image. The filter computes the weighted sum of the digital number (DN) values within the kernel surrounding each pixel. The smoothed image provides the enlargement of building boundaries and decreases the difference between the DN values of the pixels. Smoothing was necessary to increase the possibility of detecting the shadow edges as connected pixels. Next, a Prewitt edge-detection filter was applied on the Gaussian filtered image to detect the shadow casting edges of the buildings. The Prewitt edge-detection filter generates an image where sharp changes in DN values are shown. In the filtered image higher DN values indicate the presence of an edge between two features.

A critical element of the edge detection procedure was deciding where to place a threshold boundary to extract those pixels corresponding to shadow edges and to eliminate the noisy pixels from further processing. To find the optimum threshold, 130 well-distributed samples were selected from the edge pixels of 40 buildings. An equal amount of samples (65) was collected from the edge pixels of 20 collapsed and 20 uncollapsed buildings. When collecting the samples care was taken to select minimum 1 and maximum 4 samples from each of the selected buildings. For collapsed buildings, the mean value and standard deviation were computed as 23.5 and 13.5 (8 bits) respectively. The low mean value would indicate the absence of the cast shadows due to collapse. For uncollapsed buildings, the mean value and standard deviation were found to be 92.40 and 22.88, respectively. The high mean value computed for uncollapsed buildings would be considered due to cast shadows. The distribution curves for the samples collected are illustrated in figure 3. By analysing figure 3 the threshold boundary was identified as 52, which is the intersection of the two curves. Therefore, pixels with a DN value of 52 and below were considered to represent the shadow edges of those buildings collapsed due to earthquake. Similarly, those pixels with a DN value above 52 were accepted as belonging to shadow edges of uncollapsed buildings. The digital orthophoto, the Prewitt edge-filtered image, and the thresholded edge image of a highly damaged urban area are illustrated in figure 4(*a*), (*b*) and (*c*), respectively, with the vector

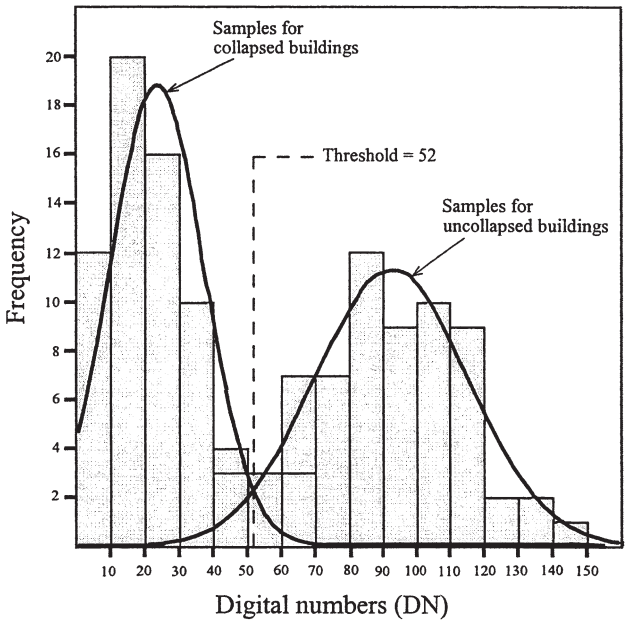

Figure 3. The distribution curves for the samples collected from the edge pixels of collapsed and uncollapsed buildings.

building polygons overlaid. The effect of the earthquake is clearly visible in figure 4. There is a remarkable difference in cast shadows between collapsed and uncollapsed buildings.

5.2. *Detection of shadow-casting edges*

Shadow edges were detected using a simple set of image-processing techniques including the Sun angle determination and shifting the building polygons in the illumination direction by an amount of one pixel in order to detect those edges that cast shadows. Figure 5(*a*) and (*b*) shows a cast shadow, where an uncollapsed building blocks direct solar illumination from reaching the ground. The width of the shadow, measured along the direction of the Sun, depends on the Sun elevation and the height of the building. As can be known, the differences in DN values, between a shadow area and its surroudings, are large. Therefore, we need to identify the shadow-casting edges of the buildings, and then apply analysis techniques to determine whether a building being considered is collapsed or not. The shadow cast by an uncollapsed building forms a shadow region. The Prewitt edge filtering applied earlier on the digital orthophoto extracted no edges from collapsed buildings for they do not cast shadows and extracted two edges from cast shadows of uncollapsed buildings. Of the two edges extracted for uncollapsed buildings, one corresponds to the boundary between the cast shadow and the surroundings on the ground and the other corresponds to the boundary between the shadow and the building. In the present case the boundary between the cast shadow and the building was used for assessing the condition of a building (figure 5(*b*)). The shadow-detection technique assumes parallel projection of the Sun's rays. The Sun angle was measured as the angle between the east direction and the direction of the illumination. To do that an uncollapsed building with

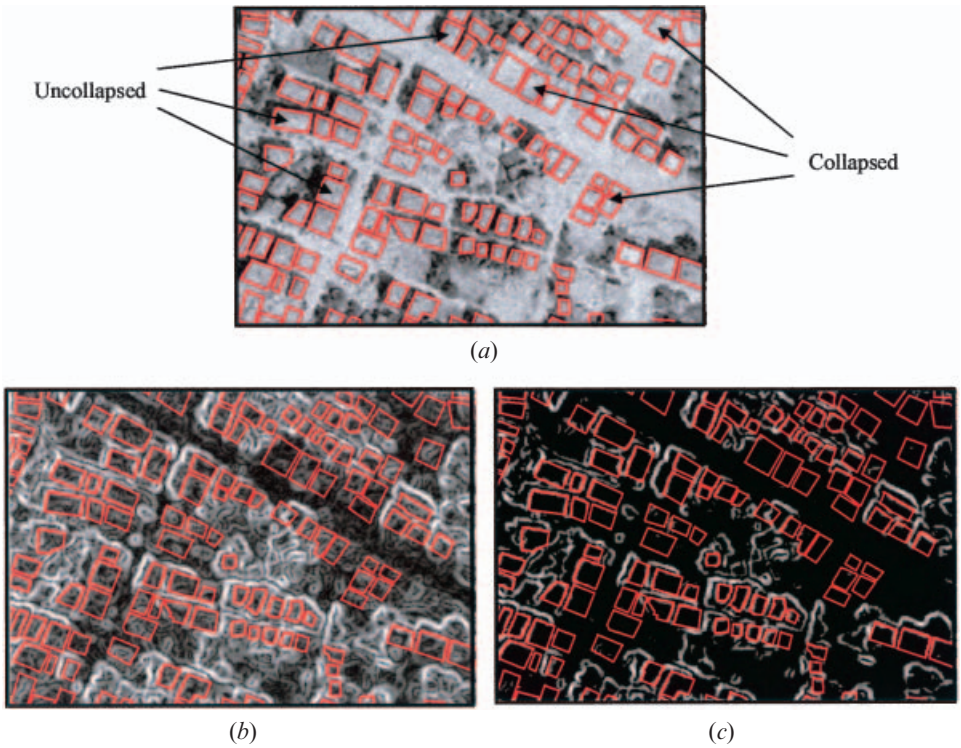

Figure 4. (*a*) The digital orthophoto, (*b*) the Prewitt edge-filtered image, and (*c*) the thresholded edge image of a hard-hit urban area.

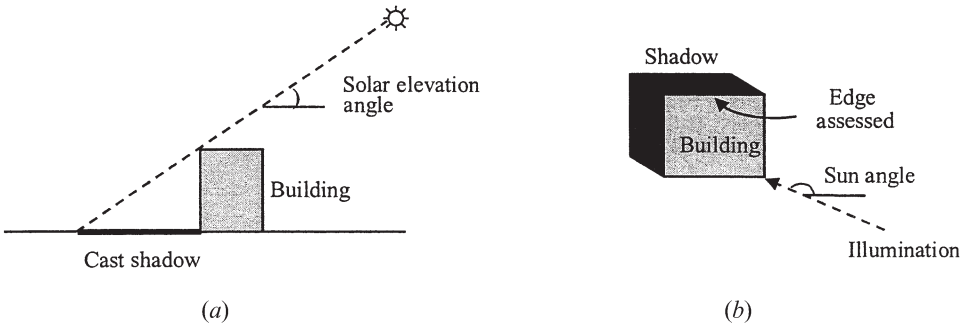

Figure 5. (*a*) Illustration of a cast shadow, where an uncollapsed building blocks direct solar illumination from reaching the ground. (*b*) Sun orientation, shadow area and the shadow casting edges.

well-defined casting shadows was used. A line, which passes over a sharp corner on the building and the corresponding shadow corner on the ground, was drawn. We then estimated the Sun angle on the digital orthophoto at 135° from the east direction.

After finding the Sun angle, this angle was utilized to identify those edges of the buildings that produce shadows. The evaluation of the condition of a building was carried out based on the shadow producing edges only. The shadow-producing

edges were identified using a simple logic developed for this study. The logic works well for rectangular-shape buildings where roof shadows are parallel to the roof edges. The complex-shape buildings, such as the S-shape, O-shape and the like, may not provide satisfactory results. Therefore, we do not claim that our logic is valid for all shapes of buildings. This logic meets the requirements for identifying the shadow casting edges of rectangular-shape buildings. On the other hand, the study area consists mainly of rectangular-shape buildings.

To identify the shadow producing edges, we utilized the building polygons which were digitized from 1 : 5000-scale paper map and stored in vector form in the database. For each polygon, a unique polygon identification number and the corner points (nodes) belonging to the polygon were also stored in the database. Therefore, we were able to identify those edges that intersect at a node of interest through a database query. In order to detect the shadow-casting edges of a building polygon, we shift the polygon along the Sun's illumination direction and search for a node of the original polygon that falls within the shifted polygon. Those edges that intersect at the node falling inside the shifted polygon are then labelled shadow-producing edges (figure 6(*a*)). In an extreme case, two nodes of the original polygon may fall on those edges of the shifted polygon that are exactly oriented in the Sun's illumination direction. In such a case, the edge that starts and stops at these two nodes is labelled the shadow-casting edge (figure 6(*b*)).

5.3. *Detection of collapsed buildings*

The detection of collapsed buildings was performed using the integrated dataset of Prewitt edge-filtered image and the vector polygon layer. The integration between the two data layers is necessary to carry out the assessments in a building-specific manner. The building-based assessment has an advantage for detecting the collapsed buildings through analysis of their shadow-producing edges. There are many edge pixels that fall outside the shadow edges of the buildings. However, these pixels are not included in the assessment of the building polygons. Therefore, the edge pixels falling outside the building polygons do not affect the assessment results.

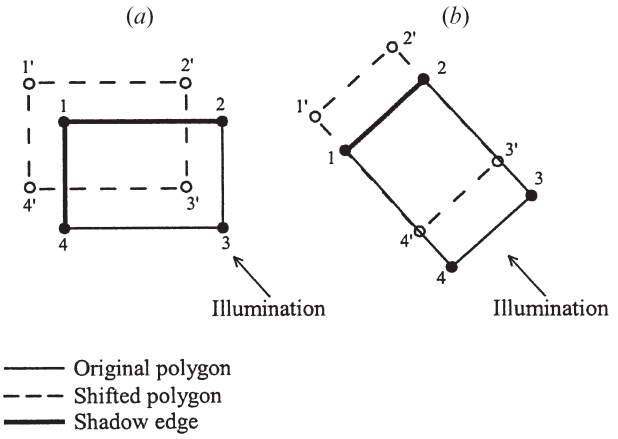

Figure 6. Illustration identifying the shadow casting edges: (*a*) shadow-casting edges are incident to node 1 which falls within the shifted polygon; and (*b*) shadow-casting edge connects nodes 1 and 2.

The building polygons were retrieved one-by-one through a database query. For each polygon, the shadow-casting edges were identified by using above given logic. These edges were converted into a raster object and overlaid on the thresholded edge image. The agreement was then measured between the shadow-producing edges of each building polygon and the thresholded edge image. To do this, a pixel count was initiated to determine the percentage of shadow edge pixels. Ideally, the shadow edges of collapsed buildings should contain low percentages. Similarly, the shadow edges of uncollapsed buildings should contain high percentages of shadow edge pixels. In reality, these may not be the cases, however. Figure 7 illustrates the thresholded edge image of a small area with the vector building polygons overlaid. A close agreement is evident between the shadow-casting edges of uncollapsed buildings (numbers 37, 38, 39 and 43 in figure 7) and the corresponding shadow edge pixels. On the contrary, the absence of shadow information indicates that the building is collapsed (numbers 41 and 42 in figure 7).

In the present case the threshold, which refers to the optimum percentage for separating the collapsed from uncollapsed buildings, was found using a method proposed by Fung and LeDrew (1988). A threshold value of 30% was chosen in the first iteration. In the subsequent iterations, it was increased with an increment of 5% at each stage until the threshold value of 70% was reached. The results obtained at each iteration were assessed with the reference data. Error matrices were produced and analysed for each threshold value. The optimum threshold was identified as 50%, which provided the overall accuracy of 96.15%. If the computed percentage value was below 50% then the building being assessed was declared as collapsed. Polygons with a percentage value above this threshold were labelled uncollapsed. Table 1 illustrates a typical error matrix generated using the optimum threshold value of 50%.

The accuracy indices generated from the error matrix include the producer's accuracy, the user's accuracy, the overall accuracy, the average accuracy, the combined accuracy and the Kappa coefficient of agreement (K). The average accuracy is an average of the accuracy of individual categories. It can be computed as either the user's accuracy or the producer's accuracy. The combined accuracy is the average of the overall accuracy and average accuracy. It can also be computed in both ways (Fung and LeDrew 1988). These accuracy indices were computed at

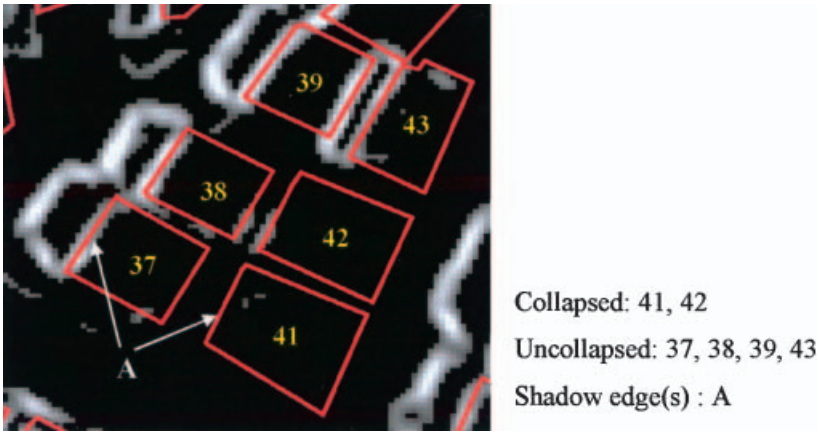

Figure 7. A thresholded edge image of a small area with the vector-building polygons overlaid.

Table 1. Error matrix of the optimum threshold value of 50%.

Analysed data		Reference: Collapsed	Reference: Uncollapsed	Total
Collapsed		74	12	86
Uncollapsed		6	375	381
Total		80	387	467
Producer's accuracy	:	92.50	96.90	
User's accuracy	:	86.05	98.42	
Average accuracy (producer's)	:			94.70
Average accuracy (user's)	:			92.24
Overall accuracy	:			96.15
Combined accuracy (producer's)	:			95.42
Combined accuracy (user's)	:			94.19
Overall Kappa ($\times 100$)	:			86.82

each iteration. Table 2 presents the changing pattern of the accuracy indices as the threshold value changes at every 5% increment. This is also illustrated graphically in figure 8.

6. Results and discussion

The four accuracy indices, namely overall accuracy, overall Kappa, combined user's accuracy and combined producer's accuracy, exhibit a common property (table 2). As the threshold value increases, these four accuracy indices also increase towards a maximum at the threshold value of 50%, after which they then decrease. The average user's accuracy and average producer's accuracy exhibit distinctive results. While the average user's accuracy is the maximum at 35%, the highest average producer's accuracy is at 55%. However, for both indices, the highest accuracies are not significantly different from the accuracies at the optimum threshold value of 50%.

The results are indeed quite satisfactory. Both the collapsed and uncollapsed buildings were detected with a high accuracy. As can be observed in table 2, the 50% threshold value for detecting collapsed buildings from the edge image has the

Table 2. The accuracy indices computed for the threshold values between 30% and 70%.

Threshold (%)	Overall accuracy (%)	Overall Kappa $\times 100$	Average accuracy: User's	Average accuracy: Producer's	Combined accuracy: User's	Combined accuracy: Producer's
30	95.289	83.072	92.417	90.712	93.853	93.001
35	95.717	84.765	**92.817**	91.962	94.267	93.840
40	95.717	85.064	92.124	92.954	93.921	94.336
45	95.931	86.017	92.025	94.075	93.978	95.003
50*	**96.146**	**86.817**	92.236	94.700	**94.191**	**95.423**
55	95.289	84.485	89.889	**95.174**	92.589	95.232
60	94.433	81.997	88.234	94.658	91.333	94.545
65	92.934	78.050	85.565	94.249	89.249	93.591
70	92.077	75.812	84.263	93.732	88.170	92.905

*The optimum threshold level based on overall accuracy, overall Kappa, combined user's accuracy, and combined producer's accuracy.

Figures in bold represent the highest accuracy.

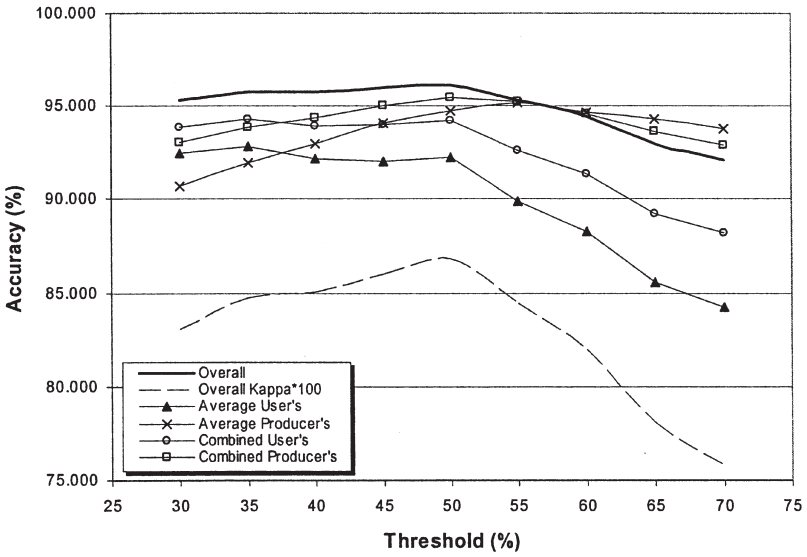

Figure 8. Illustration of the changing pattern of the accuracy indices as the threshold value changes at every 5% increment.

highest Kappa coefficient of 0.8682. In addition, the 50% threshold value also has the highest overall accuracy of 96.15%, the highest combined user's accuracy of 94.19%, and the highest combined producer's accuracy of 95.42%. Therefore, in the present case, 50% was selected as the optimum threshold value.

The automatic detection of the collapsed buildings through digital analysis of post-earthquake aerial photographs based on shadow information is quite encouraging. As expected, the approach developed and implemented in this study successfully detected the collapsed buildings caused by the earthquake. The results of the analysis achieved using the optimum threshold value of 50% illustrates a high degree of agreement with the reference data (table 1). This is also illustrated graphically in figure 9 where the collapsed buildings are illustrated in red, while the blue and green coloured buildings correspond to commission and omission errors, respectively. Of the total 467 buildings analysed, 449 (the sum of the elements along the major diagonal) were correctly categorized as collapsed and uncollapsed, providing an overall accuracy of 96.15%. A high degree of agreement is evident between the analysis results and the reference data for collapsed buildings. Of the 80 collapsed buildings, 74 were correctly detected, providing 92.5% producer's and 86.05% user's accuracies. Six buildings were omitted from this category. A high degree of agreement is also observed between the analysis results and the reference data for uncollapsed buildings. Of the 387 buildings labelled uncollapsed through the analyses, 375 agree with the reference data.

A further investigation was carried out to determine what might have caused those collapsed and uncollapsed buildings to deviate from reference data. The condition of each of the wrongly categorized buildings was carefully inspected on the digital orthophoto through visual analysis. It was found that the approach did not work properly in several cases. In the first case, an uncollapsed building casts shadows on a closely located other building. Therefore, the shadow-casting edges of the building polygon do not match with the corresponding shadow edges. For example, the uncollapsed buildings numbers 25, 91, 195, 349, 361, 383, 390, 434 and

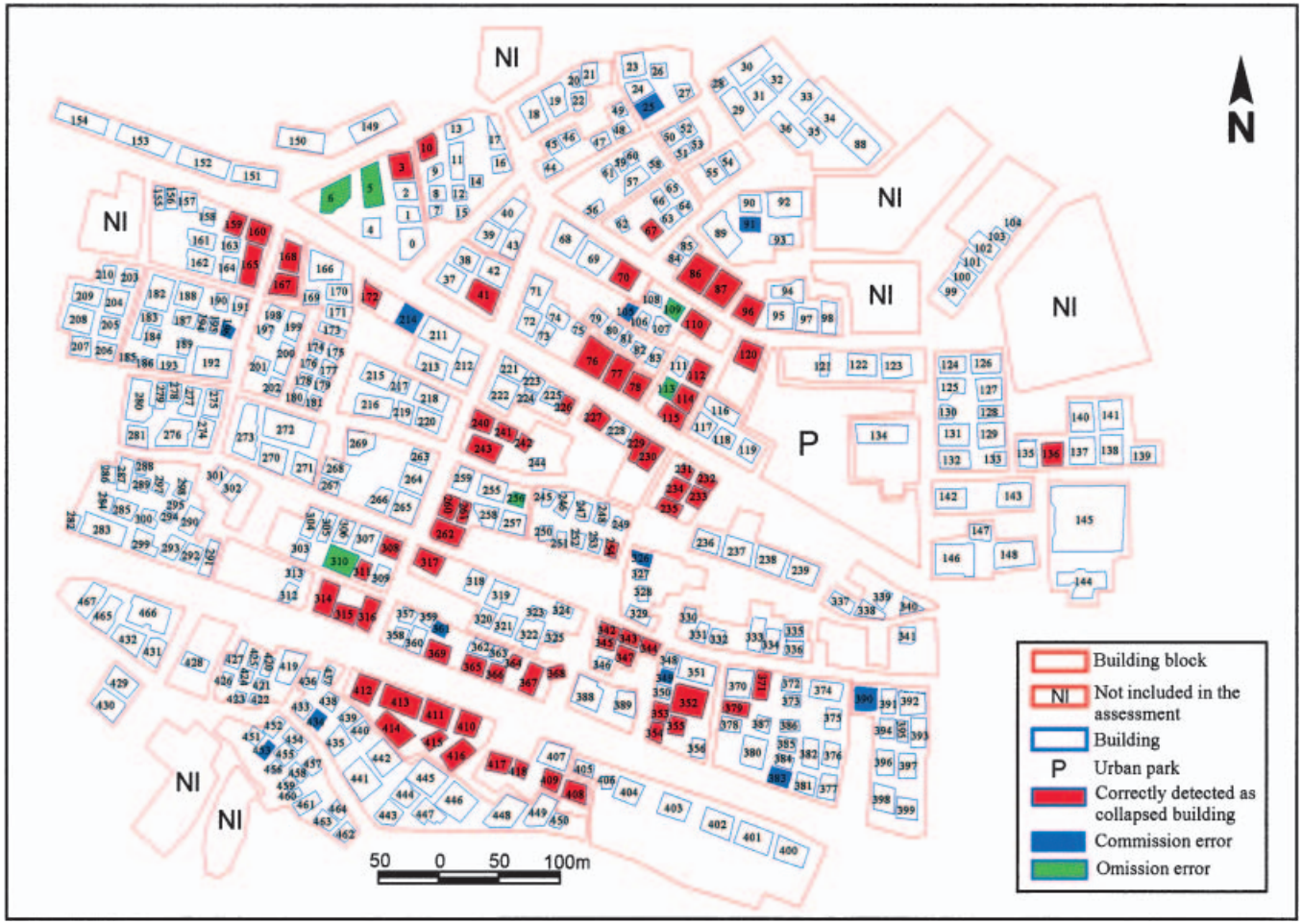

Figure 9. Illustration of the results of the analyses.

453 were erroneously detected as collapsed due to this reason. A similar confusion was also observed for building 214, which was wrongly categorized as collapsed although the reference data suggest that this building is uncollapsed. It is evident on the building polygon layer that there is no closely located building on which building 214 can cast a shadow. However, when we carefully checked the digital orthophoto we observed that there is a building located very closely to building 214. It appears that this building was constructed between the date of the compilation of the maps (1998), which is before the earthquake, and the date of aerial photo acquisition (1999), after the earthquake.

In the second case, the vegetation near the shadow casting edges of an uncollapsed building causes confusion. When compared with the brighter tone of the collapsed buildings, the vegetated areas have a much lower reflectance and appear darker than the surrounding objects. Therefore, the edge pixels generated by the Prewitt edge-detection filter correspond to sharp changes in DN values between the collapsed building and the vegetation near the building. This causes the collapsed buildings to be labelled incorrectly as uncollapsed. For example, it is clearly evident on reference data that building 310 is collapsed. However, this building was erroneously labelled uncollapsed due to the above reason. The confusion caused by the vegetation was also observed in the opposite direction. Buildings 105 and 326 were detected as collapsed although they were uncollapsed. The investigation showed that the Prewitt edge-detection filter did not accentuate the shadow casting edges of these buildings. It was observed that the computed percentage value fell below the preset threshold of 50% and therefore these two buildings were erroneously labelled collapsed.

In the third case, the building does not collapse completely and therefore casts shadows. Although the width of the shadows along the Sun's illumination direction is narrower than that of uncollapsed buildings, these shadows cause the wrong categorization of the building. For example, the reference data suggest that building 256 did not collapse completely. However, because this partially collapsed building casts shadows, it was therefore erroneously labelled uncollapsed. Similarly, building 113 was improperly labelled uncollapsed. The investigation showed that the rubble of this building produced shadows which seem to have caused the erroneous labelling of the building.

7. Conclusions

In this study, we presented the detection of the collapsed buildings caused by the Izmit, Turkey earthquake of 17 August 1999 through digital analysis of the post-event aerial photographs. We showed how the relationship between the buildings and the cast shadows can be exploited to detect collapsed buildings due to earthquake. The results of the analysis reveal that cast shadows can provide very useful cues for detecting the collapsed buildings. The results are quite encouraging. Of the 80 collapsed buildings, 74 were detected correctly, providing 92.50% producer's accuracy. A high degree of agreement is also evident between the analysis results and the reference data for uncollapsed buildings. Of the 387 uncollapsed buildings, 375 were labelled correctly, providing 96.90% producer's accuracy. The overall accuracy was found to be 96.15%.

It is important to determine the optimum threshold for separating shadow edge pixels of collapsed buildings from those of uncollapsed buildings. In this study, the threshold DN value was found to be 52. It is also quite important to determine the optimum percentage for the edge pixels of shadow-casting edges in order to

successfully separate collapsed from uncollapsed buildings. In the present case the optimum threshold value was identified as 50%. These threshold values are valid for this study only, and should not be considered universal. The building-based analysis logic performed in this study has an advantage. For each building, only the corresponding shadow edge pixels are included in the analysis of the building considered. Therefore, the analysis results are not affected by those pixels that fall outside the building polygons.

Our approach has several shortcomings to be improved in the future. The identification of the shadow-casting edges of complex-shape buildings is one problem. Our logic meets the requirements for identifying shadow-casting edges of rectangular-shape buildings. The other problem is the detection of collapsed buildings located quite close to vegetation. Satisfactory results may also not be obtained from those buildings casting shadows on another building.

Acknowledgments

The authors are grateful to General Command of Mapping for providing the post-earthquake digital orthophoto covering the study area to conduct this research.

References

FUNG, T., and LEDREW, E., 1988, The determination of optimal threshold levels for change detection using various accuracy indices. *Photogrammetric Engineering and Remote Sensing*, **54**, 1449–1454.

GAMBA, P., and CASCIATI, F., 1998, GIS and image understanding for near-real-time earthquake damage assessment. *Photogrammetric Engineering and Remote Sensing*, **64**, 987–994.

GUPTA, R. P., SARAF, A. K., SAXENA, P., and CHANDER, R., 1994, IRS detection of surface effects of the Uttarkashi earthquake of 20 October 1991, Himalaya. *International Journal of Remote Sensing*, **15**, 2153–2156.

HUERTAS, A., and NEVATIA, R., 1988, Detecting buildings in aerial images. *Computer Vision, Graphics, and Image Processing*, **41**, 131–152.

IRVIN, R. B., and MCKEOWN, D. M., 1989, Methods for exploiting the relationship between buildings and their shadows in aerial imagery. *IEEE Transactions on Systems, Man, and Cybernetics*, **19**, 1564–1575.

LETTIS, W., BACHHUBER, J., WITTER, R., BARKA, A., BRAY, J., PAGE, W., and SWAN, F., 2000, Surface fault rupture. *Earthquake Spectra* **16** (suppl. A), 11–53.

LIN, C., HUERTAS, A., and NEVATIA, R., 1994, Detection of buildings using perceptual grouping and shadows. *Proceedings of IEEE Computer Science Conference on Computer Vision and Pattern Recognition, Seattle, Washington, USA, 21–23 June*, pp. 62–69.

LIOW, Y., and PAVLIDIS, T., 1990, Use of shadows for extracting buildings in aerial images. *Computer Vision, Graphics, and Image Processing*, **49**, 242–277.

PCI, 2002, *Software Users Manual* (PCI Geomatics: Ontario, Canada).

SARAF, A. K., SINVHAL, A., SINVHAL, H., GHOSH, P., and SARMA, P., 2002, Satellite data reveals 26 January 2001 Kutch earthquake-induced ground changes and appearance of water bodies. *International Journal of Remote Sensing*, **23**, 1749–1756.

SINGH, R. P., BHOI, S., and SAHOO, A. K., 2002, Changes observed in land and ocean after Gujarat earthquake of 26 January 2001 using IRS data. *International Journal of Remote Sensing*, **23**, 3123–3128.

TURKER, M., and CETINKAYA, B. accepted, Automatic detection of earthquake damaged buildings using DEMs created from pre- and post-earthquake stereo aerial photographs. *International Journal of Remote Sensing*.

TURKER, M., and SAN, B. T., 2003, SPOT HRV data analysis for detecting earthquake-induced changes in Izmit, Turkey. *International Journal of Remote Sensing*, **24**, 2439–2450.